Pharm Res (2014) 31:1418–1425
DOI 10.1007/s11095-013-1142-0

RESEARCH PAPER

Biocompatible Glycol Chitosan-Coated Gold Nanoparticles for Tumor-Targeting CT Imaging

In-Cheol Sun • Jin Hee Na • Seo Young Jeong • Dong-Eog Kim • Ick Chan Kwon • Kuiwon Choi • Cheol-Hee Ahn • Kwangmeyung Kim

Received: 4 January 2013 / Accepted: 1 July 2013 / Published online: 9 August 2013

ABSTRACT

Purpose The application of gold nanoparticles (AuNPs) in biomedical field was limited due to the low stability in the biological condition. Herein, to enhance stability and tumor targeting ability of AuNPs, their surface was modified with biocompatible glycol chitosan (GC) and the *in vivo* biodistribution of GC coated AuNPs (GC-AuNPs) were studied through computed tomography (CT).

Methods Polymer-coated gold nanoparticles were produced using GC as a reducing agent and a stabilizer. Their feasibility in biomedical application was explored through CT in tumor-bearing mice.

Results Stability of gold nanoparticles increased in the physiological condition due to the GC coating layer on the surface. Tomographic images of tumor were successfully obtained in the tumor-xenografted animal model when the GC-AuNPs were used as a CT contrast agent. The tumor targeting property of the gold nanoparticles was due to the properties of GC because GC-AuNPs were accumulated in the tumor, while most of heparin-coated nanoparticles were found in the liver and spleen.

Conclusions The polymer properties on the surface played an important role in the behavior of gold nanoparticles in the biological condition and the enhanced stability and tumor targeting property of nanoparticles were inherited from GC on the surface.

KEY WORDS CTcontrast agent · glycol chitosan · gold nanoparticle · tumor targeting

ABBREVIATIONS

AuNPs	Gold nanoparticles
CT	Computed tomography
EDC	1-Ethyl-3-(3-dimethylaminopropyl) carbodiimide hydrochloride
GC	Glycol chitosan
GC-AuNPs	Glycol chitosan coated gold nanoparticles
HEPA-AuNPs	Heparin coated gold nanoparticles
MTT	3-(4,5-Dimethylthiazol-2-yl)-2, 5-diphenyltetrazolium bromide
NHS	N-hydroxy succinimide
PBS	Phosphate-buffered saline
TEM	Transmission electron microscopy

INTRODUCTION

For the biomedical application, researchers have studied gold nanoparticles (AuNPs) over many years. Their unique properties such as biocompatibility have promoted the use of AuNPs in biology or clinical fields (1,2). Also their strong fluorescence absorption by resonance energy transfer (FRET) was applied for the molecular imaging probe (3,4). In addition, AuNPs were used as platform for delivery carrier

I.-C. Sun • I. C. Kwon • K. Choi • K. Kim (✉)
Center for Theragnosis, Biomedical Research Institute, Korea Institute of Science and Technology, Seoul, South Korea
e-mail: kim@kist.re.kr

J. H. Na • S. Y. Jeong
Department of Life and Nanopharmaceutical Sciences, Kyung Hee University, Seoul, South Korea

D.-E. Kim
Department of Neurology, Dongguk University, Goyang, South Korea

I. C. Kwon
KU-KIST School, Korea University, Seoul, South Korea

C.-H. Ahn (✉)
Engineering Research Institute (ERI), Department of Materials Science and Engineering, Seoul National University, Seoul, South Korea
e-mail: chahn@snu.ac.kr

(5,6), or therapeutic agents (7,8) because their surface can be easily modified with simple chemistry. Nevertheless, the application of bare AuNPs was limited due to the low stability in the physiological condition. To overcome the limitation, the surface was modified with various polymers such as PEG (9), heparin (10) and chitosan (11) to enhance the stability. Those biocompatible polymers played an important role in the enhanced stability and additional functionality in the biological condition. However, the influence of the polymers on the behavior of AuNPs in the body has not been clearly studied yet, even though the properties of coating polymers are critical. Only the effects of particle size (12,13), surface charge (14), or molecular weight of polymers (15) on cellular uptake have been reported.

In this study, we developed the tumor targeting AuNPs through surface modification with glycol chitosan (GC). GC is a derivate of chitosan with improved hydrophilicity, which is obtained from N-deacetylation of chitin (16). GC was selected as a coating material because it has been well known for its biocompatibility and tumor targeting property (17,18) and frequently used in various biomedical application such as drug delivery, siRNA carrier, cancer imaging, and therapy (19–22). We expected the synergic effect of GC-coated AuNPs (GC-AuNPs), which inherited tumor targeting property and biocompatibility from the GC on the surface. The selective accumulation of AuNPs in the tumor tissue was applied to a CT contrast agent for cancer imaging. Their characteristics and the behavior in the biological condition were compared with that of heparin-coated AuNPs (HEPA-AuNPs), which our group has reported previously (10), to understand the role of GC in the tumor targeting property of GC-AuNPs in tumor-bearing mice.

Among the several imaging techniques, computed tomography (CT) was used to study the tumor targeting properties of GC-AuNP. CT has been used clinically because of unlimited penetration depth and high spatial resolution. In addition, AuNPs can be used as a CT contrast agent with low toxicity, high X-ray absorption coefficient, and slow clearance in the body (23). Hence, it was suggested that AuNPs could overcome the drawbacks of an iodine-based CT contrast agent, which has renal toxicity and fast excretion (24). Moreover, CT does not require any additional labeling in contrast to other imaging techniques such as positron emission tomography (PET) and optical imaging. It is crucial in assessment of properties of nanoparticles because other materials introduced on the nanoparticles can alter the properties of polymers and nanoparticles. For this reason, CT imaging was used to visualize the cancer using GC-AuNPs and analyze the behavior of the nanoparticles in the body.

MATERIALS AND METHODS

Materials

Gold(III) chloride trihydrate($HAuCl_4 \cdot 3H_2O$, 99%), glycol chitosan (GC, degree of deacetylation = 82.7%; MW = 250,000), and 1-Ethyl-3-(3-dimethylaminopropyl) carbodiimide hydrochloride (EDC) were purchased from Sigma (St. Louis, MO, USA). N-hydroxy succinimide (NHS; 98%) was obtained from Aldrich (Milwaukee, WI, USA). Water used in the experiment was double-distilled and all other chemicals were used as received without any purification.

Instruments

Centrifugation of AuNPs was performed in Micro 17TR (Hanil, Korea) with 2-ml Eppendorf tubes at 10,000 rpm for 10 min. The TEM images were acquired from JEM-3010 (JEOL, Japan) operating at 300 kV. 10 μl of AuNP colloid was dropped on carbon-coated, 200-mesh copper grids, followed by removing extra solution and drying in a vacuum oven for 24 h. UV–vis absorption was investigated in UV-1650PC (Shimadzu, Japan). Particle size distribution and zeta (ζ) -potential data were obtained with ELS-Z2 (Otsuka, Japan). Fourier-transform infrared (FT-IR) spectra were obtained from Spectrum GX (Perkin Elmer) on the wave number range from 4,000 to 400 cm^{-1}. GC-AuNP colloid was dried on the KBr pellets, which were prepared with the pressure of 10 t. CT images of live mice were acquired under intraperitoneal anesthesia (pentobarbital salt, 50 mg/kg) using Skyscan 1076 microCT (Skyscan Inc., Belgium) with following parameters: 70 KV, 140 μA, 35 μm of resolution, 632 ms of exposure time and 1° of rotation step.

Preparation of Polymer Coated Gold Nanoparticles

Glycol chitosan coated gold nanoparticles (GC-AuNP) were produced as previously reported (25). Briefly, 300 ml of aqueous GC solution (0.1 wt.%, w/w) was boiled to 70°C and mixed with 100 ml of $HAuCl_4 \cdot 3H_2O$ solution (1 mM) under stirring for over 24 h until solution turned from light yellow to deep red. Then, the solution was cooled down to room temperature. The colloid was centrifuged (9000 rpm, 15 min) twice with distilled-water and sonicated for less than 1 min to disperse nanoparticles uniformly.

To compare the properties of GC-AuNP, heparin coated AuNPs (HEPA-AuNP) were also made in our experiment as previously reported (10). Briefly, heparin (50 mg), EDC (5 mg) and NHS (3 mg) were dissolved in 10 ml of slightly acidic (pH = 5) water and DOPA (3 mg)

was added to the solution under stirring for 12 h. The product was purified with extensive dialysis method for 3 days. The same volume of AuNP colloid and aqueous solution of DOPA-modified heparin (0.2 wt.% w/w) were mixed and stirred for 6 h. The colloid was centrifuged (9,000 rpm, 15 min) twice with distilled-water and sonicated for less than 1 min to disperse nanoparticles uniformly.

Cytotoxicity (MTT Assay)

The cytotoxicity was determined through MTT colorimetric procedure. HeLa cells (obtained from ATCC, Rockville, MD, USA) were seeded at a density of 2×10^4 cells/well in 96-well flat-bottomed plates (SPL Life Sciences, Seoul, Korea) and allowed to adhere in DMEM medium (WelGENE, Daegu, Korea) containing 10% (v/v) FBS (Gibco, Grand Island, NY) and 1% (W/V) penicillin/streptomycin at 37°C in a humidified atmosphere of 5% CO_2 for 24 h. The cells were washed twice with phosphate-buffered saline (PBS) and exposed to various concentrations of citrate-reduced AuNP, GC-AuNP from 0.036 to 1.8 mg/ml. After 24 h, the medium was aspirated and the cells were washed twice with PBS to remove excess nanoparticles. Then 0.5 mg/ml of MTT solution in fresh medium was added and incubated for another 2 h at 37°C. The media were removed and the blue formazan crystals were dissolved in DMSO. Before colorimetric measurement, the dissolved solutions were transferred to Eppendorf tubes and centrifuged to remove precipitated citrate-reduced AuNPs. It was due to their instability when they were exposed to culture medium. Ultraviolet absorbance at 570 nm was measured with a microplate reader (VERSAMAXTM, Molecular Devices Corp., Sunnyvale, CA) and the data were expressed as the percentages of viable cells compared to the control group.

Cellular Uptake

Murine macrophage cells (RAW264.7) and murine colon cancer cells (CT-26) were obtained from the American Type Culture Collection (Manassas, VA), respectively. CT-26 were cultured in DMEM (Gibco, Grand Island, NY, USA) media and RAW264.7 in RPMI 1640 (Gibco, Grand Island, NY, USA) containing 10% fetal bovine serum (FBS; Invitrogen Canada, Burlington, ON, Canada), 100 U/ml penicillin G, and 100 mg/ml streptomycin. For microscopic examination cells were seeded at a density of 2×10^4 cells onto 15 mm gelatin-coated cover slips in 12-well plates and allowed to grow until a confluence of 70−80%. Prior to the experiment, cells were washed twice with PBS (pH 7.4) to remove the remnant growth medium, and then incubated for 30 min in serum-free medium containing AuNPs (0.05 mg Au/ml). The cells were then washed twice with cold PBS (pH 7.4), fixed with fresh 4% paraformaldehyde for 5 min at room temperature, and mounted with Fluoromount-G™ (SouthernBiotech, Birmingham, AL). The intracellular localization of nanoparticles was observed using IX81-ZDC focus drift compensating microscope (Olympus, Tokyo, Japan) equipped with a dark-field condenser.

Liver Metastasis Animal Model

CT-26 colon cancer cells were cultured in Dubecco's modified Eagle's medium (DMEM, Gibco, Grand Island, NY) containing 10% (v/v) FBS (Gibco) and 1% (W/V) penicillin/streptomycin at 37°C in a humidified atmosphere of 5% CO_2. C3H/HeN mice (5.5 weeks, male) were anesthetized with ketamine (80 mg/kg body weight) and xylazine (10 mg/kg body weight) by intraperitoneal injection. After anesthesia, laparotomy was performed with direct injection of CT-26 cancer cells (3×10^5 cells) in 10 μl of saline into left lobe in the liver. CT images of the live mice were obtained after 10 days of colon cancer transplantation.

CT Imaging

For CT image study, AuNPs were concentrated up to 50 mg Au/ml before injection. After injection (100 μl) to CT-26 tumor bearing mice through tail vein, the mice were scanned by *in vivo* micro-computed tomography (Skyscan 1076, Skyscan Inc., Belgium) under intraperitoneal anesthesia (pentobarbital salt, 50 mg/kg) with following parameters: 70 KV, 140 μA, 35 μm of resolution, 632 ms of exposure time and 1° of rotation step. CT images were taken before injection, 30 min, 1 h and 24 h after injection.

Scheme 1 Chemical structure of glycol chitosan (GC) and surface-modified AuNPs (GC-AuNP).

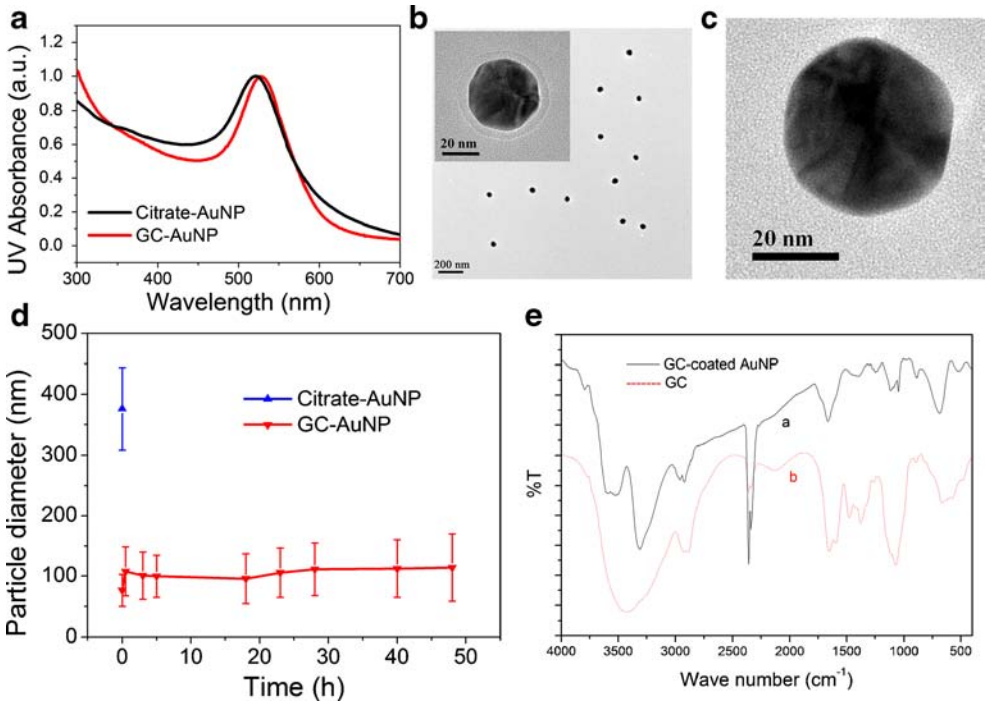

Fig. 1 (**a**) UV–vis spectrum of citrate-reduced AuNP and GC-AuNP. (**b**) TEM images of GC-AuNP (inset : magnified images). (**c**) citrate reduced AuNP. (**d**) Stability of AuNP and GC-AuNP in physiological condition (PBS) measured with DLS. (**e**) FT-IR spectra of GC-AuNP and GC.

Histology

The dissected liver tissues with metastatic cancer were retrieved and fixed in 4% (v/v) buffered formalin solution, dehydrated and embedded in paraffin. Sections were cut with thickness of 6 mm and stained with hematoxylin and eosin (H&E). The samples were observed through IX81 microscope (Olympus) equipped with a dark-field condenser.

RESULTS AND DISCUSSION

Characterization of GC-AuNPs

Conventional method of AuNP synthesis was reduction of $HAuCl_4$ with sodium citrate. However, the citrate-stabilized AuNPs are not appropriate for the biological purpose due to their lack of stability in the presence of salt. To enhance the stability and biocompatibility of AuNPs in the biological condition, we used GC as a reducing agent and a stabilizer in the $HAuCl_4$ solution during the AuNP formation instead of sodium citrate (Scheme 1). In addition, it has been known that GC nanoparticles have an excellent tumor targeting property in various tumor-bearing mice (22). Therefore, we expected that the use of GC also promote the selective accumulation of AuNPs in the tumor.

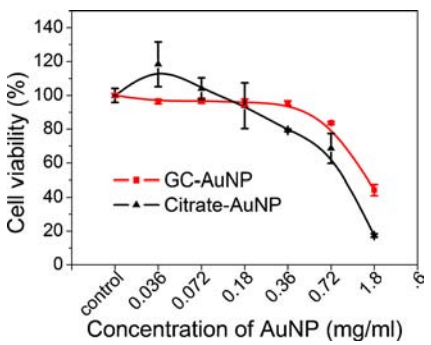

Fig. 2 Cell viability after incubation for 24 h with AuNP and GC-AuNP.

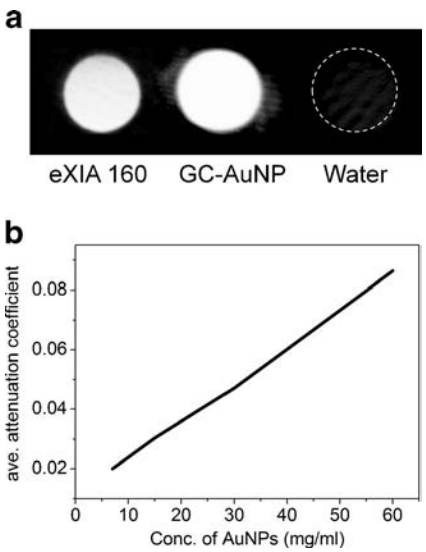

Fig. 3 (**a**) *In vitro* microCT images of eXIA™ 160, GC-AuNP (60 mg/ml) and water. (**b**) Averaged attenuation coefficient of GC-AuNP as a function of concentration.

UV–vis spectroscopy revealed that the surface plasmon resonance (SPR) peak of GC-AuNPs wasslightly red-shifted from 521 to 526 nm (Fig. 1a). This indicated successful surface modification of AuNPs because the polymer layer changed refractive index around AuNPs (26,27). In addition, polymer coating layer was observed around GC-AuNPs in the transmission electron microscopy (TEM) images (Fig. 1b), while the citrate reduced AuNPs showed no layers (Fig. 1c). Monodispersed spherical GC-AuNPs with the diameter of approx. 20 nm were clearly seen without aggregation in the TEM images. It was also confirmed with dynamic light scattering (DLS). Without polymer coating, the particle size in the colloid state was 24.0±6.2 nm, which was almost the same with that in an anhydrous state (TEM images). However, the diameter of GC-AuNPs increased up to 99.4±16.8 nm due to the hydrated expansion of the polymer layer in aqueous state, even though the core size was almost similar with that of citrate-reduced AuNPs as shown in TEM images. This result showed that the hydrodynamic volume of AuNPs can be changed significantly because of the GC polymer properties on the surface. The surface charge of AuNPs measured with zeta (ζ) potential analyzer also reflected the properties of polymers. ζ-potential of GC-AuNPs was positive (+34.48±1.0 mV) because of electropositive amine groups of GC (28), while that of citrate-reduced AuNPs was −26.0±0.4 mV. The existence of GC on the AuNPs' surface was also confirmed with Fourier-transform infrared (FT-IR) spectroscopy. The broad peak at 3,310 cm^{-1} (bonded NH or NH_2) and at 1,405 cm^{-1} (primary amine) were the evidence of GC on the surface of AuNPs (29), since the new peaks of amine groups was observed (Fig. 1e). In particular, the stability and biocompatibility of GC-AuNPs in physiological condition should be guaranteed for the biomedical application. For this reason, the diameter of GC-AuNPs in PBS buffer solution was monitored to evaluate their stability before cellular experiment. As shown in Fig. 1d, GC-AuNPs maintained their sizes more than 2 days in the buffer condition due to the enhanced stability caused by encapsulation with GC. On the other hand, the particle diameter of uncoated AuNPs appeared as a point, because aggregation occurred as soon as they were exposed to PBS. Therefore, it was not possible to keep track of its size any longer. In addition, we checked the stability of GC-AuNP under mild acidic condition (pH=3) in our previous work (data not shown), which guaranteed the integrity of GC-

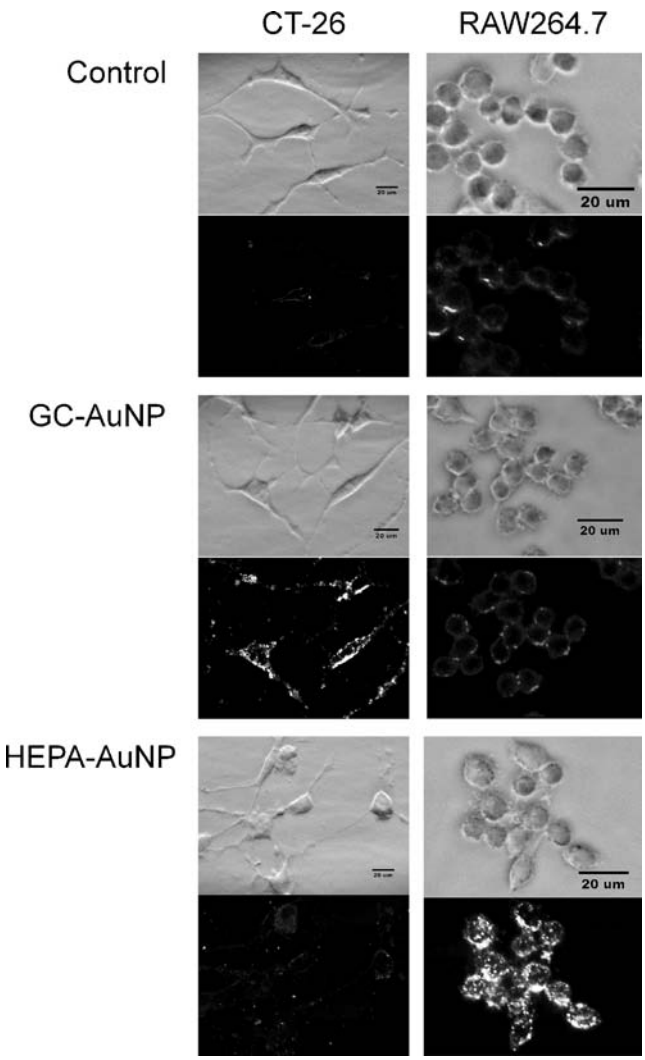

Fig. 4 Dark-field microscopic images of CT-26 (colon cancer cells) and RAW264.7 (macrophage) after 30 min of incubation with GC-AuNP and HEPA-AuNP.

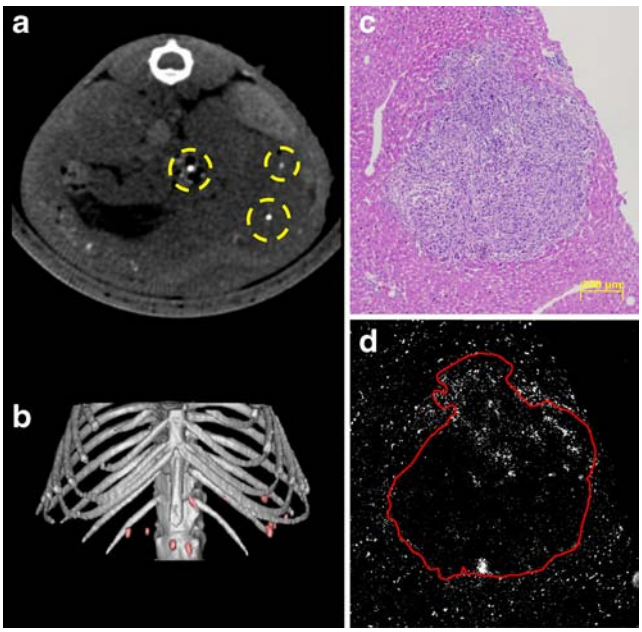

Fig. 5 (**a**) Cross sectional CT images and (**b**) its reconstructed 3D images of liver with colorectal metastases after 30 min of intravenous injection of GC-AuNP. (**c**) Histological images of CT-26 colon cancer in liver after 2 h of treatment with GC-AuNP and (**d**) its dark-field image.

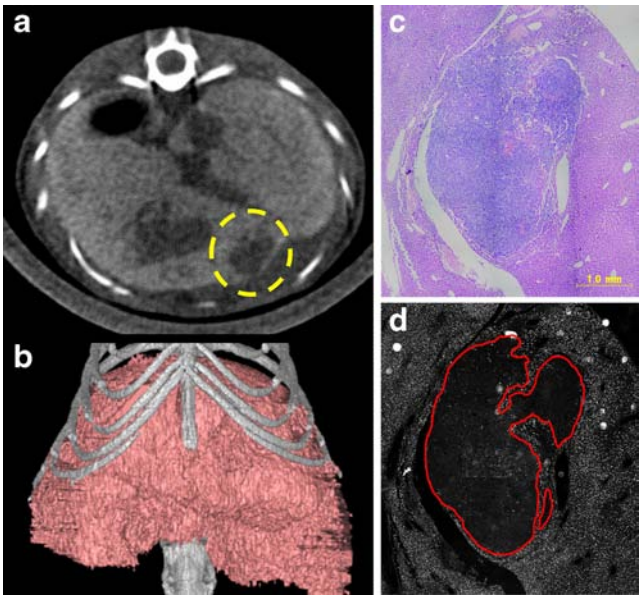

Fig. 6 (**a**) Cross sectional CT images and (**b**) its reconstructed 3D images of liver with colorectal metastases after 30 min of intravenous injection of HEPA-AuNP (**c**) Histological images of CT-26 colon cancer in liver after 2 h of treatment with HEPA-AuNP and (**d**) its dark-field image.

AuNPs in the tumor (25). Biocompatibility of GC-AuNPs was confirmed through MTT assay (Fig. 2). When HeLa cells were incubated for 24 h with GC-AuNPs, severe toxicity was not observed and cell viability were slightly higher than that of uncoated AuNPs. Consequently, the stability and biocompatibility were significantly improved by the GC coating layer on the surface, which ensure their application in biomedical field.

Feasibility of GC-AuNPs as a CT Contrast Agent

It has been reported that AuNPs can absorb not only visible light but also X-ray. Moreover, AuNPs can overcome the disadvantages of iodine-based contrast agent due to the low toxicity, slow clearance and higher X-ray absorption coefficient (9,23,24). For this reason, the feasibility of GC-AuNPs as a CT contrast agent was tested for CT imaging study with them. GC-AuNPs were concentrated up to 50 mg Au/ml to maximize X-ray absorption and their phantom CT images of test tubes were compared with that of eXIA™ 160 (commercial CT contrast agent) and water (Fig. 3a). The phantom images were highly contrasted with GC-AuNPs, which were comparable to that of commercial CT contrast agent. In addition, X-ray absorption increased linearly according to the concentration of GC-AuNP (Fig. 3b). It also increased according to concentration regardless of their polymer coating layers on the surface when it was compared with heparin coated AuNPs (HEPA-AuNPs), which our group previously reported (10). This result suggested that only Au atom is responsible for X-ray absorption, and their surface properties did not affect it. Therefore, CT imaging can be used to monitor the behavior of polymer-coated AuNPs in the body without interference of X-ray absorption from the polymers on the AuNP surface.

Selective Internalization of AuNPs According to Cell Lines and Surface Properties

The behavior of GC-AuNPs in cellular level was explored using two types of cells, i.e. colon cancer cells (CT-26) and macrophage cells (RAW264.7). The two cell lines were chosen because they clearly showed different aspect of cellular uptake and the tumor targeting property of GC-AuNPs. They were incubated for 30 min with GC-AuNPs and intracellular localization of nanoparticles was observed through dark-field microscopy. As shown in Fig. 4, they did not show a strong signal in the dark-field microscopy before they were exposed to AuNPs (denoted as control). However, GC-AuNPs were found exclusively in CT-26 colon cancer cells, not in macrophage cells. The selective uptake of GC-AuNPs in cancer cells was due to the tumor targeting properties of GC on the surface of AuNPs. It was reported that pKa value of GC (pKa≈6.5) induced positive charges of amine functional groups in acidic microenvironment of tumor tissues (30). Because of that, GC-coated nanoparticles were thought to be easily internalized in cancer cells.

To examine the tumor targeting property of GC-AuNPs more thoroughly, AuNPs with different surface properties was also used in cellular uptake. Previously, we developed liver-targeting AuNPs using heparin as a coating material

Table I Attenuation Coefficient of HEPA-AuNP and GC-AuNP in Liver, Heart, Spleen and Metastatic Cancer (tumor) According to Injection Time

	HEPA-AuNP				GC-AuNP			
	30 min	60 min	120 min	24 h	30 min	60 min	120 min	24 h
Liver	1.148	1.167	1.166	1.101	0.953	1.053	1.061	0.887
Heart	0.920	0.983	0.945	0.955	0.983	1.148	1.022	0.978
Spleen	1.138	1.237	1.583	1.445	1.107	1.226	1.272	1.130
Tumor	0.887	0.894	0.838	0.812	1.577	2.043	2.060	1.170

* Hundredth ($\times 10^{-2}$)

(HEPA-AuNP), which selectively accumulated in the normal liver tissue, not in the tumor. According to the previous works, heparin promotes uptake of AuNPs by the reticulo-endothelial system and the endothelial cells in the liver (10,31). As seen in Fig. 4, the signals of HEPA-AuNPs were observed only in RAW264.7 macrophage cells. In short, heparin increased cellular uptake of HEPA-AuNPs in macrophage cells, while GC boosted that of GC-AuNPs in cancerous cells. Therefore, the tumor targeting property of GC-AuNP was endowed by GC on the surface and the polymer properties on the surface made a different aspect of the particles' behavior in the biological environment.

CT Imaging of Tumor with GC-AuNPs

Using GC-AuNPs as a tumor targeting CT contrast agent, positive-contrasted tumor imaging was possible in metastatic liver cancer model. Colorectal liver metastasis was induced by direct injection of CT-26 colon cancer cells in the liver. GC-AuNPs were selectively accumulated in the tumor within 30 min when GC-AuNPs (0.1 ml, 50 mg Au/ml) were injected intravenously into the CT-26 tumor bearing mice (150~200 mg Au/kg). Consequently, positively contrasted CT image of the tumor tissue was obtained in Fig. 5a, which was coincided with the cellular uptake result. Moreover, the tumor specific GC-AuNPs revealed several tumor sites spread over the liver simultaneously, as seen in the reconstructed 3D image of liver with metastatic cancer (Fig. 5b). This result indicated that the tumor targeting property of GC-AuNPs was so sensitive and efficient that even small tumors (< 0.6 mm) in various locations were able to be detected at the same time. For further investigation, the mice were sacrificed and analyzed histologically. The liver tissues with metastatic cancers were excised and stained with H&E to observe through optical and dark-field microscope. Tumors were easily distinguished from the normal liver tissue by H&E staining (Fig. 5c). It provided more information on the tumor specific accumulation of GC-AuNPs when they were overlapped with dark-field images. GC-AuNPs were found inside the tumor tissue and the signals from normal liver tissue was relatively weak (Fig. 5d). Due to the insensitivity of dark-field microscopy, the detected signal from GC-AuNPs in the tumor did not perfectly coincide with that of the CT image. However, we confirmed that the enhanced CT contrast of tumor was achieved by gold nanoparticles, not by tumor tissue itself. In addition, some NPs were observed outside of the tumor in the dark-field microscopic image. It was thought that the high vascularity of tumor caused GC-AuNPs to remain around tumor tissue, due to their enhanced stability and the long circulation (32).

When the same amount of HEPA-AuNPs was injected intravenously, cancer was negatively contrasted in the cross sectional CT image after 30 min (Fig. 6a and b). It is due to the selective accumulation of HEPA-AuNPs in the Kupffer cells, which were widely distributed in the normal tissue. It was reported that reduced number of macrophage, especially Kupffer cells leads the increment of metastasis (33,34). In other words, HEPA-AuNPs did not internalize in the tumor tissue even though the diameter of tumor was more than 2 mm because of decreased Kupffer cells in the tumor. It was also confirmed with dark-field microscopic images of liver cancer. Scattered light signals from HEPA-AuNPs were detected only from the hepatocytes, not from the CT-26 cancer tissues (Fig. 6c and d).

The different surface properties of nanoparticles resulted in a disparate aspect of biodistribution as well. After injection of HEPA-AuNPs and GC-AuNPs into the tumor bearing mice, the attenuation coefficients in major tissues were summarized in Table I. The table demonstrated that HEPA-AuNPs were accumulated in the spleen and liver, while most of GC-AuNPs in the tumor. This result also proved that the properties of polymers on the surface of AuNPs determined the different aspect of biodistribution. In this study, we showed that GC-AuNPs with tumor targeting property was able to be applied in the medical field as a CT contrast agent. Moreover, it provided accurate anatomical data of the metastatic liver cancer in the CT images. Therefore, our GC-AuNP showed its potential as a tumor specific CT contrast agent for cancer imaging. In addition, the abundant amine groups of GC-AuNPs provide many sites for chemical conjugation of anti-cancer drugs, which would open up possibilities that GC-AuNPs may be developed as a multifunctional platform for cancer imaging and therapy.

CONCLUSION

Tumor targeting GC-AuNPs were produced through surface modification with biocompatible polymers. They were characterized with TEM images, UV–vis absorption spectra, ζ-potential, and DLS. They showed excellent stability, biocompatibility, and enhanced tumor accumulation. These properties were inherited from GC on the surface, which were distinguished from that of HEPA-AuNPs. These properties were applied to CT image of tumors. Several tumor sites of metastatic liver cancer were successfully located in the CT images, which were also confirmed with histological analysis and dark-field microscopy.

ACKNOWLEDGMENTS AND DISCLOSURES

In-Cheol Sun and Jin Hee Na contributed equally to this work. This work was financially supported by the Intramural Research Program of KIST, GRL Program, and M.D.-Ph.D. Program (2010–0019863, 2010–0019864).

REFERENCES

1. Daniel MC, Astruc D. Gold nanoparticles: assembly, supramolecular chemistry, quantum-size-related properties, and applications toward biology, catalysis, and nanotechnology. Chem Rev. 2004;104(1):293–346.
2. Murphy CJ, Gole AM, Stone JW, Sisco PN, Alkilany AM, Goldsmith EC, *et al.* Gold nanoparticles in biology: beyond toxicity to cellular imaging. Acc Chem Res. 2008;41(12):1721–30.
3. Lee S, Cha EJ, Park K, Lee SY, Hong JK, Sun IC, *et al.* A near-infrared-fluorescence-quenched gold-nanoparticle imaging probe for in vivo drug screening and protease activity determination. Angew Chem Int Ed. 2008;47(15):2804–7.
4. Mu CJ, LaVan DA, Langer RS, Zetter BR. Self-assembled gold nanoparticle molecular probes for detecting proteolytic activity in vivo. Acs Nano. 2010;4(3):1511–20.
5. Paciotti GF, Myer L, Weinreich D, Goia D, Pavel N, McLaughlin RE, *et al.* Colloidal gold: a novel nanoparticle vector for tumor directed drug delivery. Drug Deliv. 2004;11(3):169–83.
6. Ganesh T. Improved biochemical strategies for targeted delivery of taxoids. Bioorg Med Chem. 2007;15(11):3597–623.
7. Haba Y, Kojima C, Harada A, Ura T, Horinaka H, Kono K. Preparation of poly(ethylene glycol)-modified poly(amido amine) dendrimers encapsulating gold nanoparticles and their heat-generating ability. Langmuir. 2007;23(10):5243–6.
8. Pitsillides CM, Joe EK, Wei XB, Anderson RR, Lin CP. Selective cell targeting with light-absorbing microparticles and nanoparticles. Biophys J. 2003;84(6):4023–32.
9. Kim D, Park S, Lee JH, Jeong YY, Jon S. Antibiofouling polymer-coated gold nanoparticles as a contrast agent for in vivo x-ray computed tomography imaging. J Am Chem Soc. 2007;129(24):7661–5.
10. Sun IC, Eun DK, Na JH, Lee S, Kim IJ, Youn IC, *et al.* Heparin-coated gold nanoparticles for liver-specific CT imaging. Chem Eur J. 2009;15(48):13341–7.
11. Bhumkar DR, Joshi HM, Sastry M, Pokharkar VB. Chitosan reduced gold nanoparticles as novel carriers for transmucosal delivery of insulin. Pharm Res. 2007;24(8):1415–26.
12. De Jong WH, Hagens WI, Krystek P, Burger MC, Sips AJAM, Geertsma RE. Particle size-dependent organ distribution of gold nanoparticles after intravenous administration. Biomaterials. 2008;29(12):1912–9.
13. Chithrani BD, Ghazani AA, Chan WCW. Determining the size and shape dependence of gold nanoparticle uptake into mammalian cells. Nano Lett. 2006;6(4):662–8.
14. Kim B, Han G, Toley BJ, Kim CK, Rotello VM, Forbes NS. Tuning payload delivery in tumour cylindroids using gold nanoparticles. Nat Nanotechnol. 2010;5(6):465–72.
15. Zhang GD, Yang Z, Lu W, Zhang R, Huang Q, Tian M, *et al.* Influence of anchoring ligands and particle size on the colloidal stability and in vivo biodistribution of polyethylene glycol-coated gold nanoparticles in tumor-xenografted mice. Biomaterials. 2009;30(10):1928–36.
16. Desai KGH, Park HJ. Preparation and characterization of drug-loaded chitosan-tripolyphosphate microspheres by spray drying. Drug Dev Res. 2005;64(2):114–28.
17. Zhang Y, Zhang MQ. Calcium phosphate/chitosan composite scaffolds for controlled in vitro antibiotic drug release. J Biomed Mater Res. 2002;62(3):378–86.
18. Na JH, Lee SY, Lee S, Koo H, Min KH, Jeong SY, *et al.* Effect of the stability and deformability of self-assembled glycol chitosan nanoparticles on tumor-targeting efficiency. J Control Release: Off J Controlled Release Soc. 2012;163(1):2–9.
19. Huh MS, Lee SY, Park S, Lee S, Chung H, Lee S, *et al.* Tumor-homing glycol chitosan/polyethylenimine nanoparticles for the systemic delivery of siRNA in tumor-bearing mice. J Control Release: Off J Controlled Release Soc. 2010;144(2):134–43.
20. Kim JH, Kim YS, Park K, Kang E, Lee S, Nam HY, *et al.* Self-assembled glycol chitosan nanoparticles for the sustained and prolonged delivery of antiangiogenic small peptide drugs in cancer therapy. Biomaterials. 2008;29(12):1920–30.
21. Lee SJ, Koo H, Jeong H, Huh MS, Choi Y, Jeong SY, *et al.* Comparative study of photosensitizer loaded and conjugated glycol chitosan nanoparticles for cancer therapy. J Control Release: Off J Controlled Release Soc. 2011;152(1):21–9.
22. Na JH, Koo H, Lee S, Min KH, Park K, Yoo H, *et al.* Real-time and non-invasive optical imaging of tumor-targeting glycol chitosan nanoparticles in various tumor models. Biomaterials. 2011;32(22):5252–61.
23. Hainfeld JF, Slatkin DN, Focella TM, Smilowitz HM. Gold nanoparticles: a new X-ray contrast agent. Br J Radiol. 2006;79(939):248–53.
24. Krause W. Liver-specific X-ray contrast agents. Top Curr Chem Contrast Agents II. 2002;222:173–200.
25. Sun IC, Eun DK, Koo H, Ko CY, Kim HS, Yi DK, *et al.* Tumor-targeting gold particles for dual computed tomography/optical cancer imaging. Angew Chem Int Ed. 2011;50(40):9348–51.
26. Underwood S, Mulvaney P. Effect of the solution refractive-index on the color of gold colloids. Langmuir. 1994;10(10):3427–30.
27. Norman TJ, Grant CD, Magana D, Zhang JZ, Liu J, Cao DL, *et al.* Near infrared optical absorption of gold nanoparticle aggregates. J Phys Chem B. 2002;106(28):7005–12.
28. Janes KA, Calvo P, Alonso MJ. Polysaccharide colloidal particles as delivery systems for macromolecules. Adv Drug Deliv Rev. 2001;47(1):83–97.
29. Wang XH, Ma JB, Wang YN, He BL. Structural characterization of phosphorylated chitosan and their applications as effective additives of calcium phosphate cements. Biomaterials. 2001;22(16):2247–55.
30. Crayton SH, Tsourkas A. pH-titratable superparamagnetic iron oxide for improved nanoparticle accumulation in acidic tumor microenvironments. Acs Nano. 2011;5(12):9592–601.
31. Hiebert L. The uptake of heparin by liver sinusoidal cells in normal and atherosclerotic rabbits. Thromb Res. 1981;21(4–5):383–90.
32. Frieboes HB, Wu M, Lowengrub J, Decuzzi P, Cristini V. A computational model for predicting nanoparticle accumulation in tumor vasculature. PLoS ONE. 2013;8(2):e56876. doi:10.1371/journal.pone.0056876.
33. Pearson HJ, Anderson J, Chamberlain J, Bell PRF. The effect of kupffer cell stimulation or depression on the development of liver metastases in the rat. Cancer Immunol Immunother. 1986;23(3):214–6.
34. Malter M, Friedrich E, Suss R. Liver as a tumor-cell killing organ - kupffer cells and natural killers. Cancer Res. 1986;46(6):3055–60.